Chemical Engineering Journal 328 (2017) 159–171

Contents lists available at ScienceDirect

Chemical Engineering Journal

journal homepage: www.elsevier.com/locate/cej

Concomitant degradation of complex organics and metals recovery from fracking wastewater: Roles of nano zerovalent iron initiated oxidation and adsorption

Olusegun K. Abass [a,b], Maoshui Zhuo [a,b], Kaisong Zhang [a,*]

[a] CAS Key Laboratory of Urban Pollutant Conversion, Institute of Urban Environment, Chinese Academy of Sciences, Xiamen 361021, China
[b] University of Chinese Academy of Sciences, Beijing 100049, China

HIGHLIGHTS

- FW from Yanchang formation, Ordos Basin has very poor biodegradability.
- n-ZVI achieves simultaneous degradation of PEGs, TPHs, and FW dechlorination.
- Processes controlling degradation/removal of TPH and PEGs by n-ZVI were clarified.
- XRF spectroscopy confirms recovery of metals and non-metals by n-ZVI from FW.

GRAPHICAL ABSTRACT

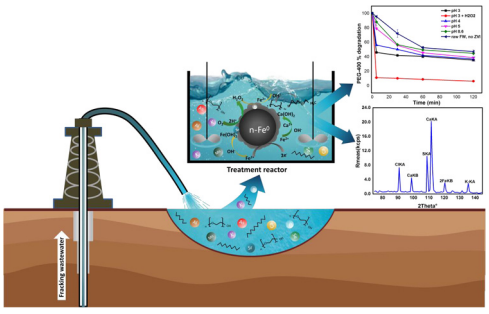

ARTICLE INFO

Article history:
Received 13 March 2017
Received in revised form 4 July 2017
Accepted 5 July 2017
Available online 6 July 2017

Keywords:
Fracking wastewater
Polyethylene glycols
Degradation pathway
Metals recovery
Total petroleum hydrocarbon
Nano zerovalent iron

ABSTRACT

This work examines the characteristics of fracking wastewater from an emerging shale play in Central China, and the catalytic activity of nano-sized zerovalent iron (n-ZVI) particles to degrade major organic components of fracking wastewater (FW), and to simultaneously recover/remove metals and potential toxic elements. Addition of optimized concentration of n-ZVI (2 g/L) to the raw FW led to COD reductions of 30% at pH 4, and 54% at pH 3 (with addition of H_2O_2) respectively within 120 min reaction time. Activity of n-ZVI catalyst on degradation kinetics of total petroleum hydrocarbon (TPH) was over 6 times faster in acidic condition (K_{rc} = 0.0029 min^{-1}), than at natural pH of the raw FW (K_{rc} = 0.00046 min^{-1}). Meanwhile, oxidant-assisted degradation of the FW TPH reached higher degradation amounts (C/C_0 = 0.191) at half the time required for treatment without oxidant addition (C/C_0 = 0.218), and thus, implies a reduce treatment cost at shorter reaction time. Moreover, n-ZVI initiated oxidation led to rapid degradation of the FW polyethylene glycols (93.7% PEGs removal), as verified by liquid chromatography/-tandem triple quadrupole mass spectrometry (LC–MS/MS), and possible degradation pathway of PEGs by n-ZVI was deduced. Similarly, n-ZVI recover metals and remove potential halocarbon-forming elements like chlorine as confirmed by X-ray fluorescence (XRF) analysis. Furthermore, the n-ZVI catalyst essentially increased biodegradability index of the FW at lower pH, and in the presence of oxidants. Therefore, pre-treatment of FW with n-ZVI represents a potential and cost-effective treatment option for the reuse of fracking wastewaters.

* Corresponding author.
E-mail address: kszhang@iue.ac.cn (K. Zhang).

http://dx.doi.org/10.1016/j.cej.2017.07.030
1385-8947/

1. Introduction

Despite the strain on China's water resources, the country continues to tap into the vast potentials of its water-intensive unconventional oil and gas development. In the US, oil and gas production through the process of hydraulic fracturing, otherwise known as fracking is expected to increase by 45% from 24.4 trillion cubic feet (Tcf) in 2013, to 35.5 Tcf by 2040 [1]. While in China, which holds the world largest technically recoverable shale plays (1275 Tcf) envisage to increase production by 8–12% in 2020, from the nearly 0.23 (Tcf) output in 2015 according to the National 12th five year plan for Shale gas development. Fracking is also employed in the UK and over a dozen countries on main land Europe, while Canada and Australia are two of the increasing number of countries trialing the technology.

The process of high-volume fracking requires the injection of several million liters of water at high pressure to fracture target formation and stimulate the shale reservoir permeability [2]. Following well completion, a portion ranging from 5% to over 100% of the fracture fluid returns and is referred to as 'produced water' which is highly contaminated and requires treatment [2,3]. Fracking fluid typically contains 99% water and sand, with the remaining 1% comprising chemical additives used to regulate pH and viscosity, and also for friction, and scaling reduction, and biocides (including formaldehyde or glutaraldehyde) for reducing biological fouling [4,5]. Similarly, water from fracking may also contain elevated levels of dissolved solids (TDS) that range from 5 to over 30 g/L, with large quantities of poorly defined organics [6]. Besides, a more challenging feature of this class of wastewater is sometimes the high concentrations of metals (such as sodium, aluminum, calcium, barium, and strontium), toxic heavy metals, bromide and naturally occurring radioactive materials (NORM) [5,7].

Due to the propriety nature of fracking fluid, along with the known nasty chemical components [5], it is not surprising that treatment of fracking wastewater (FW) presents a huge challenge and concern in regions where fracking is employed. High contents of chemicals including metals and heavy metals (such as, strontium and zinc) employed during the fracking process can become potential contaminants on reaction with chromium (used as cross-linking agents) if introduced into the environment without adequate treatment [8]. Current technologies for removing these contaminants, including coagulation-adsorption [9], biological treatment [10], and membrane filtration processes [11] all holds great promises, but are energy demanding and the resultant wastes are difficult and expensive to dispose [12]. Besides, most conventional wastewater treatment facilities are generally incapable of removing heavy metals and recalcitrant organics principally due to their non-biodegradability [13]. Therefore, treatment and reuse of FW is imperative to long-term viability of the fracking process especially in already water-stressed areas. Also, the recovery and reuse of metals from FW represents an important economic and energy cut, while reducing the amount of recalcitrant discharges into the environment.

Meanwhile, zerovalent iron (ZVI) is an environment friendly nanoparticle which is also ubiquitous. Currently, there has been a major interest in employing nanoscale zerovalent iron (n-ZVI) as electron donors for reductive/oxidative degradation of complex organics including haloalkanes [14], emerging endocrine disrupting chemicals such as bisphenol A [15], and as adsorbent/reductant for removal of chromium, arsenic, selenium, phosphate, radionuclides, and rare earth elements by either creating access to the elemental core chemistry of ZVI, or through the process of oxidative adsorption initiated by iron oxides/hydroxides formation around the shell structure during corrosion of the ZVI core [16–20]. Other contaminant removal pathways of ZVI nanoparticles include coprecipitation with iron, and iron dissolution [19,21]. Wastewater treatment with n-ZVI is becoming a widely accepted, energy saving, affordable and scalable technology suitable for commercialization [22].

In the presence of oxygen, ZVI (Fe^0) can react to generate a four electron iron oxidation process as shown in Eq. (1).

$$2Fe^0 + O_2 + 4H^+ \rightarrow 2Fe^{2+} + 2H_2O \quad (1)$$

The reaction could follow a different reaction pathway in the absence of oxygen to release Fe^{2+} and hydroxyl ions in aqueous conditions (Eq. (2)). Moreover, under acidic and oxic conditions, the reaction can proceed with the generation of hydrogen peroxides (Eq. (3)). However, in alkaline conditions, H_2O_2 may react with hydroxyl ions to form perhydroxyl ions as described in Eq. (4) [23].

$$Fe^0 + 2H_2O \rightarrow Fe^{2+} + H_2 + 2OH^- \quad (2)$$

$$Fe^0 + O_2 + 2H^+ \rightarrow Fe^{2+} + H_2O_2 \quad (3)$$

$$H_2O_2 + OH^- \leftrightarrow HO_2^- + H_2O \quad (4)$$

The in-situ generated hydrogen peroxide can then provoke the production of hydroxyl radicals on reaction with ferrous iron in what is commonly known as the Fenton reaction (Eq. (5)) [24], to achieve degradation of the organics in the FW.

$$Fe^{2+} + H_2O_2 \rightarrow Fe^{3+} + HO^{\cdot} + OH^- \quad (5)$$

$$R - H + HO^{\cdot} \rightarrow R^{\cdot} + H_2O \quad (6)$$

$$HO - [CH_2]_n - OH + HO^{\cdot} \rightarrow HO - [C^{\cdot}H]_n - OH + H_2O \quad (7)$$

$$R^{\cdot} + Fe^{3+} \rightarrow R^+ + Fe^{2+} \quad (8)$$

$$Fe^{3+} + H_2O_2 \rightarrow FeOOH^{2+} + H^+ \quad (9)$$

The hydroxyl radical (a non-selective and highly reactive oxidant) produced is capable of abstracting hydrogen atoms from organic pollutants such as TPH and PEGs (represented by R–H and HO–$[CH_2]_n^-$OH) following the general equation described in Eqs. (6) and (7) [25,26]. Therefore, increased generation of HO· will enhance the degradation of the organic components of the wastewater. The internal radical (R·) produced could react with ferric ions to release secondary ferrous iron (Eq. (8)) for the catalysis of hydrogen peroxide produced in-situ in the n-ZVI/O_2 system, and thus enable a recycling of the Fe^{2+} and promote the generation of hydroxyl radicals. However, Fe^{3+} produced as a result of oxidation of Fe^{2+} might react with hydrogen peroxide to generate Fe-oxyhydroxides (Eq. (9)), which could be a limiting step for sustained Fe^{3+}/Fe^{2+} recycle [27].

$$Fe^{2+} + H_2O_2 \rightarrow FeO^{2+} + H_2O \quad (10)$$

$$FeO^{2+} + H_2O \rightarrow Fe^{3+} + HO^{\cdot} \quad (11)$$

The regenerated Fe^{2+} described in Eq. (8) may react with H_2O_2 generated in-situ to form ferryl ion species (FeO^{2+}) due to pH elevation Eq. (10). The generation of FeO^{2+} in aqueous solution have been reported to occur at near neutral or alkaline pH due to its stability at this pH range [28,29]. Its less reactivity compared to hydroxyl radicals is due its preference for oxidized products other than saturated equivalents [30]. Ferryl ions can also react with H_2O molecules to form Fe^{3+} and hydroxyl radicals as described in Eq. (11) [31].

$$4Fe^0 + 3O_2 + 6H_2O \rightarrow 4Fe^{3+} + 12OH^- \quad (12)$$

$$2Fe^{2+} + 4OH^- \rightarrow 2Fe(OH)_2 \rightarrow 2FeO + 2H_2O \quad (13)$$

$$4Fe^{3+} + 12OH^- \rightarrow 4Fe(OH)_3 \rightarrow 2Fe_2O_3 + 6H_2O \quad (14)$$

$$3Fe^{2+} + O_2 + 2H_2O \rightarrow Fe_3O_4 + 4H^+ \quad (15)$$

$$4Fe_3O_4 + O_2 + 18H_2O \rightarrow 12Fe(OH)_3 \quad (16)$$

Other important processes occurring during the dissolution of Fe^{2+} from n-ZVI in aqueous solution is the formation of oxides/hydroxides of Fe. Generally as pH increases, the eluted Fe^{2+} is rapidly oxidized to Fe^{3+} while both Fe^{2+} and Fe^{3+} go into reaction with hydroxide ions release in solution at less acidic pH to form iron oxides/hydroxides, for removal of both inorganic and organic pollutants by precipitation, co-precipitation and adsorption as described in Eqs. (1216) [18–20,32]. A thorough understanding of these mechanisms would be valuable for treatment optimization of fracking wastewater using n-ZVI.

To this end, this work examines the characteristics of fracking wastewater from an emerging shale play in Central China, and explores the catalytic and redox properties of ZVI nanoparticles to address the challenges affecting the reclamation and reuse of fracking wastewaters with complex organic matrices and elemental compositional chemistry. Water quality indicators used to assess the treatment capacity of n-ZVI for the fracking wastewater include; chemical oxygen demand (COD), total organic carbon (TOC), total petroleum hydrocarbons (TPH) – as majority of the organic compounds identified in FW are the saturated group [33]; polyethylene glycols (PEGs) – a sequence of non-ionic polyhydroxyl compounds that are water soluble and a common component marker for FW [34]; and biodegradability using the BOD_5/COD index.

Although there have been reports on the successful use of n-ZVI for contaminants degradation/removal in various types of synthetic and industrial wastewaters [17,35,36], its application for fracking wastewater treatment is rarely found in the literature. To the best of our knowledge, this is the first time n-ZVI will be employed for simultaneous degradation of complex organics, and recovery/removal of metals and potential halocarbon-forming elements from real fracking wastewater. Possible mechanism regarding the degradation of the FW organics was described, and a brief economic assessment of the treatment system was evaluated. Ultimately, the result of this work will provide valuable knowledge for the low-cost pre-treatment of FW effluent incorporating reactive nanomaterials, primarily n-ZVI, to enhance the FW biodegradability, and possibly create room for sustainable operation of the water intensive fracking process in regions already known to be water-stressed.

2. Materials and methods

2.1. Fracking wastewater characteristics

The fracking wastewater from the shale play of Yanchang formation located in southeastern Ordos Basin of the Changqing Oil and Gas Province was generously supplied by a local giant petroleum company (Yanchang Petroleum (Group) Co. ltd, Shaanxi), which serve as intermediary to bigger players such as the state-owned oil giant CNOOC (China National Offshore Oil Corporation). The as-received wastewater were flowback waters produced during the stimulation of the shale gas well from Yanchang formation, Central China [37], and stored on-site in a retention tank before being retrieved for the experiment. The wastewater has a characteristic foaming condition when mildly agitated or even more extreme, when air is bubbled through it. This is probably due to the presence of nitrogenous based compounds, which are sourced from the gas well clean-up additives, or linear alkylbenzenesulfonates and gas frothers used in the fracking process. Conditions as this could cause the iron nanoparticles to be attached to the froth layer and consequently affecting the smooth operation of treatment reactors especially when air is applied. Therefore, an active silicone-based antifoaming agent (Antifoam Y-30 emulsion from Sigma-Aldrich) was added to all samples to avoid interference during the experiment.

2.2. Chemicals

The n-ZVI powder (99.9% metal basis, Mw 55.84 g/mol, average particle size 100 nm) used in this study was purchased from Aladdin Chemical Co. (Shanghai, China). Other physicochemical characteristics of the as-received n-ZVI powder determined by BET surface area analyzer (Micromeritics ASAP 2020) are presented in Table S1 of the Supplementary Information (SI). HPLC-grade dichloromethane (DCM) was purchased from Tedia (Fairfield, OH, USA). LiChrosolv gradient grade methanol and acetonitrile were purchased from EMD Millipore Corporation (Billerica, MA, USA). Total petroleum hydrocarbon (TPH) and o-terphenyl standards were obtained from Sigma-Aldrich (Bellefonte, PA, USA). Polyethylene glycol (PEG 400) and n-tricosane-d_{48} standards were obtained from Aladdin Chemical Co. (Shanghai, China) and Chiron AS (Trondheim, Norway) respectively. All other chemicals used were of analytical grade and stock solutions of those were prepared using Milli-Q water (>18 MΩ cm) from Millipore system (Texas, USA).

2.3. Experimental procedure

Continuous stirred tank reactors (CSTR) operated in batch mode using a six paddle jar tester (Model ZR4-6, Shenzhen, China) was used for the n-ZVI oxidation/adsorption test. All experiments were carried out at room temperature (23 ± 1 °C) in 1 L glass beakers. Extra care was taken to ascertain that the as-received n-ZVI were not exposed to ambient air before being introduced into the test reactors (as the elemental iron powder can spontaneously be oxidized and easily ignited on contact with air). The experiments were conducted in oxic conditions (air flow rate 1.5 L/min) with different concentrations of n-ZVI (0, 30, 45, 100, 500, 1000, 2000, 3000 mg) added to 1 L of the undiluted fracking wastewater. Samples were retrieved from the reactors' supernatant at different times, and the reaction terminated by attracting the n-ZVI particles to the base of the collection vessels via a powerful magnet. Subsequently the supernatants were filtered through 0.22 μm filters before analysis. Afterwards, an optimized n-ZVI concentration was chosen to study the role of pH and time on contaminants degradation/removal by n-ZVI. Further experiments were carried out by adjusting the pH of the FW to 4 ± 1 (using appropriate amounts of 1 M of HCl and the wastewater whose pH is 8.6 ± 0.1) At each stage of the treatment, the degradation efficiencies (DE) of the organics (TPH and PEGs) in the control (without n-ZVI), n-ZVI/O_2 and n-ZVI/O_2/H_2O_2 systems, respectively were calculated as shown in Eq. (17):

$$DE(\%) = \frac{D_i - D_f}{D_i} \times 100 \quad (17)$$

where D_i and D_f are the initial and final concentrations of TPH or PEGs in the FW before and after treatment with all systems.

2.4. Physico-chemical analysis

Chemical and biological analysis including total organic carbon (TOC), chemical oxygen demand and 5-day biological oxygen demand (COD & BOD_5) were analyzed using TOC-V_{CPH} analyzer (Shimadzu, Japan), colorimetric COD test kits (Lian-hua Tech. Co., Ltd., China), and a LH-BOD601A intelligent BOD tester (Lianhua,

China) respectively. Analysis of the inorganic ions, metals and heavy metals content of the FW was conducted using an ion chromatograph (Dionex ICS 3000), Perkin Elmer inductively coupled plasma optical emission spectrometer (ICP-OES, Optimal 7000DV), and an inductively coupled plasma mass spectrometer (ICP-MS, Agilent Tech. 7500 Series), respectively. Quantification of the total Fe ion concentration was conducted using ICP-MS, and ferrous ion concentration was determined by the 1,10-phenanthroline method [38]. Ferric ion concentrations were derived by subtracting the ferrous ion concentration from the total Fe ion concentration. The dissolved oxygen (DO) concentration was measured using a DO probe meter (Hach Company, USA).

2.5. Total petroleum hydrocarbon

The aliphatic hydrocarbon components of the FW namely total petroleum hydrocarbon (TPH) were extracted as described by Reddy and Quinn [39], and modified as follows. 5 ml of DCM were injected into 50 ml vials of the FW samples. The resulting immiscible solution were then inverted and mechanically agitated for 25 min at 180 rpm. After the shaking step, the samples were placed in a sonication bath for 10 min and afterward allowed to settle additional 6 min. The solvent layer was extracted using a solid-phase extraction (SPE) device equipped with a 5 ml packed column of anhydrous Na_2SO_4 (oven-treated at 450 °C to remove residual organics) and silanized glass wool (Sigma-Aldrich, St. Louis, USA) to ensure complete removal of water and interfering particles.

The extracts were concentrated to 1.0 ml and analyzed using an Agilent 7890A gas chromatography system coupled with a mass spectrometer detector, Agilent 5975C (GC–MS). The column used was a high resolution Agilent HP-5MS model (30.0 m × 0.25 mm × 0.25 μm). The injection volume and temperature was maintained at 1 μL and 300 °C respectively. The carrier gas (helium) pressure was 8.2317 psi in a splitless flow of 1 ml/min and the oven temperature program was run at 60 °C for 6 min, followed by a ramp up of 6 °C/min to 320 °C, and a hold at 320 °C for 20 min. TPH component concentrations of the FW samples were determined using C_8 – C_{40} alkanes calibration standard (Sigma-Aldrich, Bellefonte, PA, USA). TPH extraction efficiencies were verified by spiking the samples with deuterated tricosane (n-tricosane-d_{48}) and o-terphenyl internal standards. Both have recovery efficiencies ranging from 72.2 to 80.4% and 79.4 to 86.8% respectively. The method detection limits (MDLs) were in the range of 0.018–0.17 μg/L, while the method quantification limits (MQLs), which were evaluated based on instrument quantification limits and analytes recovery, were in the range 0.06–0.56 μg/L.

2.6. PEGs

Qualitative, and quantitative analysis of PEG oligomers were performed on an ultra-high performance liquid chromatography/-tandem triple quadrupole mass spectrometer (UHPLC–MS/MS) system consisting of a Nexera UHPLC system (Nexera X2, Shamadzu Corp., Japan) and a Triple Quad 6500 Q-trap mass spectrometer (AB Sciex, USA) equipped with a Turbo spray ion source. Prior to analysis, all samples were diluted and filtered through a 0.20 μm sterilized surfactant-free filter (Silicon Valley). Blank analyses were performed on the filters to ensure they are interference free.

Chromatographic separation was carried out with a Shim-pack XR-DOS III column (2.0 mm × 75 mm, 1.6 μm particle size, 7.5 nm pore size) maintained at 30 °C. The injected sample volume was 10 μL carried along at a flow rate of 0.25 mL/min with a binary mobile phase system. Mobile phases A and B were 0.1% formic acid in water and acetonitrile/methanol, respectively. The optimized gradient was run at 10% B and kept constant for 2 min and was linearly increased to 60% over 10 min and maintained at 60% for 1 min prior to the column re-equilibration step which lasted 2 min. The ion source settings operated at positive mode were as follows: curtain gas at 25 psi, ion spray voltage at 5.5 kV, temperature at 650 °C, ion source gas 1 and 2 at 50 and 60 °C, respectively for the LC–MS and collision gas at 9 psi for the LC–MS/MS operation. The LC–MS/MS analyses were modified in the MS/MS mode and run in the MRM mode. The accurate mass spectra were acquired within a mass range of 50–1050 m/z, while the m/z values and ion species of qualifiers and quantifiers used in the LC–MS and LC–MS/MS analysis are detailed in Lichtenegger and Rychlik [40] and Vijaya Bhaskar et al. [34], respectively. The data recorded were processed with Analyst software (version 1.6.3 AB Sciex, USA). Both the MDLs and MQLs were in the range of 0.15–1.0 ng/L, and 0.5–3.4 ng/L, respectively. All instrumental and procedural blanks were below MDLs.

2.7. Solid-phase characterization of fresh and contaminant-loaded n-ZVI

Fresh and reacted n-ZVI samples were used in the analysis. The spent n-ZVI samples were retrieved from the reactors after the reaction was complete and freeze-dried prior to analysis. X-ray diffraction analysis (XRD, PANalytical X'Pert Pro) performed in the 2θ range from 5° to 80° at X-ray generator settings of 40 mA and 40 kV were used to evaluate the crystalline phases of the n-ZVI samples and the structure of surface precipitates formed. X-ray fluorescence spectroscopy (XRF) were carried out in a ZB Axios-mAX spectrometer at spectra collection time of 300 s and tube operating current and voltage of 60 μA and 60 kV, respectively to investigate the superficial elemental composition of the n-ZVI samples. The XRF limit of determination of method was derived using n = 20 replicate determinations with a 95.4% confidence level, which yielded a minimum uncertainty value in the range of 0.00146–0.02 mg/g. Fresh and spent n-ZVI samples were also subjected to Fourier transform infrared (FTIR) measurement to verify the occurrence of organic sorption on the n-ZVI samples using FTIR spectrophotometer (Nicolet iS10, Thermo Scientific, USA). Both the fresh (control) and spent n-ZVI samples for the FTIR analysis were prepared by finely dispersing the samples in KBr powder before measurement.

3. Results and discussion

3.1. Characterization of the fracking wastewater

The major characteristics and constituents of the FW are presented in Table 1. All samples retrieved from the site possess a slightly alkaline pH 8.6 ± 0.25. The TOC values (700–1514.4 mg/L) were quite high but comparable to those obtained from the horizontally fractured well of Denver-Julesburg basin, USA [9].

The FW characteristically moderate salinity (ca. 9630 mg/L, TDS) revealed that its of non-marine origin [37]. The COD levels (ca. 2318 mg/L) and biocide content, along with other inherent recalcitrant organics aggravated the biodegradability of the wastewater, as the BOD_5/COD index yielded a value of 0.09. The most abundant TPH component of the FW falls within the carbon content range of C_{10} – C_{18} (Table 2), which are similar to the carbon content range reported for Barnett and Marcellus shale gas produced water [33]. Analysis of the FW shows the presence of PEGs oligomers with varying peak intensity. Unlike produced water, which is composed of less or no PEGs, the presence of PEGs in the FW confirms that flowback waters or fracking wastewaters are characteristically composed of PEGs, and can therefore be used to differentiate a shift from the connate produced water to the injected water [34]. Further, analytical results showed that the

Table 1
Some characteristics of the raw fracking wastewater from the fracked well.

Parameter	Analytical method	Values
Bulk parameter		
TOC (mg/L)	SM 5310B	700.4–1514.4
COD (mg/L)	EPA 5220D	1576.5–2317.5
TDS (mg/L)	SM 2450C	8640.0–9630.0
Oil & Grease (mg/L)	Spectrofluorophotometry	0.1–0.23
TPH (mg/L)	GC–MS	92.4–130.6
PEGs (mg/L)	LC-MS/MS	17.8–19.9
TSS (mg/L)	SM 2450D	80.0–110.0
VSS (mg/L)	SM 2450E	28.0–54.0
Turbidity (NTU)	HACH 2100N	78.7–90.4
Inorganic ions		mg/L
Br^-	IC	30.9–37.1
SO_4^{2-}	IC	57.5–257.3
F-	IC	4.4–82.5
Cl^-	IC	541.1–3030.2
Metals & non metals		mg/L
Mg	ICP-OES	56.4–62.0
P	ICP-OES	0.14–0.22
Ca	ICP-OES	698.2–950.7
K	ICP-OES	64.4–232.7
Na	ICP-OES	743.0–1049.1
Fe	ICP-MS	0.4–2.2
Zn	ICP-MS	0.27–1.02
Sr	ICP-MS	4.07–6.34
Al	ICP-MS	0.14–0.64
Cr	ICP-MS	0.00143–0.049
As	ICP-MS	0.0024–0.003
Mn	ICP-MS	0.082–0.87
Co	ICP-MS	0.0011–0.092
Mo	ICP-MS	0.002–0.00395
Cu	ICP-MS	0.01–0.371
Ba	ICP-MS	0.192–0.952
Se	ICP-MS	0.016–0.056

PEG – Polyethylene glycol, TPH – Total Petroleum Hydrocarbon.

Table 2
The as-received fracking wastewater TPH components mean concentrations.

Component name	Chemical formula	RT (min)	Mean concentration (ppb)
Nonane	C_9H_{20}	5.12	288.4625
Decane	$C_{10}H_{22}$	8.539	8308.82
Undecane	$C_{11}H_{24}$	12.223	266.4065
Dodecane	$C_{12}H_{26}$	14.763	33299.9
Tridecane	$C_{13}H_{28}$	17.522	546.864
Tetradecane	$C_{14}H_{30}$	19.581	13726.64
Pentadecane	$C_{15}H_{32}$	21.811	1253.225
Hexadecane	$C_{16}H_{34}$	23.834	1050.523
Heptadecane	$C_{17}H_{36}$	25.894	13570.9
Octadecane	$C_{18}H_{38}$	25.894	14811.65
Nonadecane/ Pristane	$C_{19}H_{40}$	27.574	6282.44
Eicosane/Phythane	$C_{20}H_{42}$	27.574	5793.27
Heneicosane	$C_{21}H_{44}$	30.805	768.57
Docosane	$C_{22}H_{46}$	32.218	1210.015
Tricosane	$C_{23}H_{48}$	33.803	1273.533
Tetracosane	$C_{24}H_{50}$	38.13	312.6075
Pentacosane	$C_{25}H_{52}$	39.156	1089.496
Hexacosane	$C_{26}H_{54}$	40.376	365.905
Heptacosane	$C_{27}H_{56}$	41.541	349.285
Octacosane	$C_{28}H_{58}$	42.679	509.6575
Nonacosane	$C_{29}H_{60}$	43.686	402.5125
Triacontane	$C_{30}H_{62}$	44.833	496.2775
Hentriacontane	$C_{31}H_{64}$	45.863	765.5195
Dotriacontane	$C_{32}H_{66}$	46.864	602.8995
Tritriacontane	$C_{33}H_{68}$	47.835	1195.829
Tetratriacontane	$C_{34}H_{70}$	48.788	969.735
Pentatriacontane	$C_{35}H_{72}$	49.649	747.6565
Hexatriacontane	$C_{36}H_{74}$	50.601	1472.066
Heptatriacontane	$C_{37}H_{76}$	51.982	1312.38
Octatriacontane	$C_{38}H_{78}$	53.205	1143.556
Nonatriacontane	$C_{39}H_{80}$	54.768	1475.415

FW contains a number of metals, non-metals, inorganic ions, and toxic heavy metals including Sr, Mg, Al, P, K, Cl^-, Cr, Ca, As, Se, Co and so on (Table 1). The toxic heavy metals concentrations in the FW were generally less than 1 mg/L, and were comparable to those reportedly found in flowback waters in Colorado [7]. Similarly, the arsenic concentrations (2–3 μg/L) in the FW were well below the maximum contamination limit (10 μg/L) for drinking water [42]. In a recent study by Parnell et al. [43], the release of Se and Mo into groundwater were found closely related to shale gas extraction from carboniferous shale. Moreover, according to the maximum allowable concentrations of Se (10 μg/L) in China surface waters (GB3838-2002) and in the US, 50 μg/L (maximum permitted level in drinking water) [44], the concentration of Se (ca. 56.4 μg/L) in the FW calls for serious concern.

3.2. Influence of n-ZVI concentrations on TOC removal from FW

Different concentrations of n-ZVI (0.03–3 g/L) were added to the undiluted raw FW (ca. 0.8 g/L TOC) under oxic conditions to evaluate and maximize the treatment efficiency, and also to reduce treatment cost. The air flow rate (1.5 L/min) was kept fairly constant throughout the reaction time. In the reaction, the organic degradation capacity of the n-ZVI seems to increase with time as shown in Fig. 1. This implies that the contact time of nano sized iron (basically the release of ferrous ion) with the FW is highly important for the prolonged and indirect production of reactive oxygen species (ROS) such as $HO^{\cdot}$, which are actively involved in the degradation process. The rate of dissolution of n-ZVI is largely related to the amount of particulates n-ZVI, which goes into reaction with aqueous oxygen and water to spontaneously produce Fe^{2+} and oxy/hydroxides layers of iron [45]. Adversely, the latter dissolution products typically results in rapid passivation of the n-ZVI core and consequently prevents the release of ferrous species, which are important for continued degradation/mineralization of the organic pollutants [32]. However, this isn't a complete disadvantage, as the iron oxides/hydroxides layer formed enhanced the adsorption and precipitation of other components of the FW (see Section 3.7 and 3.8).

At 2 g/L n-ZVI, the highest TOC reduction of the FW were 22%, 16% and 13%, respectively at 60 min, 30 min, and 5 min treatment time in the n-ZVI/H_2O system. Further increase in the n-ZVI concentration to 3 g/L showed no appreciable TOC reduction. Hence,

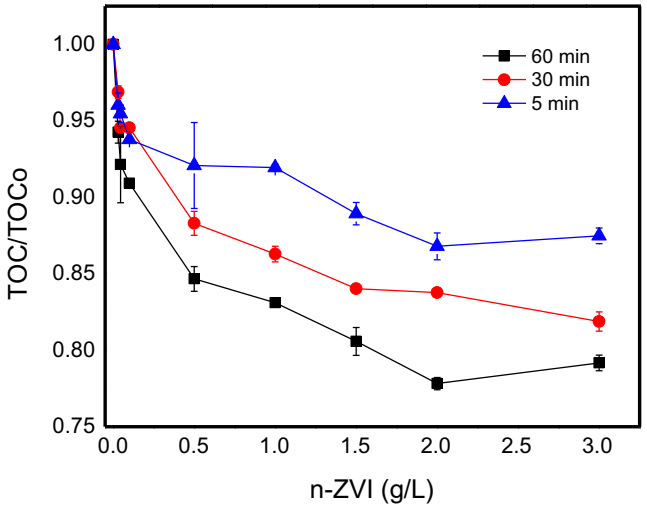

Fig. 1. Influence of n-ZVI concentration on TOC reduction of FW (at pH 4, stirring speed of 350 rpm and air flow rate of 1.5 L/min, where TOC_0 = 0.8 g/L is the initial TOC concentration of the FW without air or n-ZVI treatment).

2 g/L n-ZVI was selected as the optimized concentration for further experiments. The TOC removal of the treatment system is not efficient as higher percentage of the organics remained in the FW solution. Similarly, as shown by previous studies, treatment efficiency in terms of COD and TOC removal using advance oxidation processes (AOPs) (such as n-ZVI/H_2O_2) are relatively low for real wastewater compared to simulated ones [36,46]. Moreover, evaluating treatment index based on COD or TOC values alone can give a false conclusion on the effectiveness of a treatment process [47]. For instance, Bilińska et al. [46] compared the treatment efficiency of industrial wastewater (IW) with simulated equivalent (SW) using AOPs, and found that both the COD and TOC removal were 10 and 20% for IW, while it reached 90 and 50% for SW, respectively. Segura et al. [36] also show that the TOC removal efficiency of diluted real pharmaceutical wastewater (70%) was higher than the undiluted one (55%) at an optimum pH value of 3. In this study, the fracking wastewater was treated without dilution, which gave rise to TOC and COD reductions of 22% and 30%, respectively at pH 4. However, as shown in Table 3, the COD removal was enhanced at pH 3, with and without Fenton reagent (H_2O_2), which gave rise to higher COD reductions (see Section 3.3). The use of Fenton or Fenton-like processes for real wastewater treatment mostly goes along with the aim of oxidizing inhibitory or refractory organic compounds, and as such can be used as pretreatment step for biological processes, which can achieve complete mineralization of the oxidized products. Nevertheless, current research trend reveals that the combined use of membrane pretreatment along with Fenton or Fenton-like processes can be effective for water and wastewater treatment [18,48].

3.3. Biodegradability test

The optimized n-ZVI concentration (2 g/L) was reacted with the fracking wastewater at different pH and operating conditions to evaluate the COD removal characteristics and biodegradability (in terms of BOD_5/COD ratio). Results showed that, 48% and 30% COD conversion was achieved at pH 3 and 4, respectively, which is lesser compared to the 54% COD reduction in the reaction supplemented by H_2O_2 at pH 3 (Table 3). The biodegradability of the FW was also significantly enhanced by 15%, 47%, and 55%, respectively at pH 4, 3, and pH 3 + H_2O_2, respectively after treatment with the iron nanoparticles (Table 3). The BOD_5/COD ratio has been widely used as an approximate indicator to assess wastewater biodegradability index and was recently suggested as an important index for quantifying the efficiency of AOPs treatment systems [36,46,47,49]. However, the efficiency of the n-ZVI catalyst to essentially enhance the biodegradability of the FW at lower pH in the presence of oxidant requires further research.

3.4. TPH removal by n-ZVI and effects of pH

To understand the mechanism of TPH removal from the fracking wastewater by n-ZVI, control experiments were performed with and without the addition of n-ZVI (Fig. S1 of SI). Results showed that moderate TPH degradation occurred with continuous flow of air in the absence of n-ZVI (Fig. S1(a)). Upon addition of 2 g/L n-ZVI, significant degradation of TPH was observed from the initial 14.7% and 26.8% (without n-ZVI), to 21.0% and 50.8% (with n-ZVI) at 5 and 60 min, respectively (Fig. S1(b)). This perhaps indicates the role of n-ZVI in the degradation of TPH in FW. Kang and Hwang [24] speculated that under acidic condition (pH 3–4), hydrogen peroxide was most stable and could react more efficiently with ferrous ions to generate hydroxyl radicals (see Eq. (5)). However, at pH values greater than 5, decomposition of hydrogen peroxide was observed, which led to the deactivation of ferrous ion with attendant production of ferric hydroxo complexes.

In this study, the reduced capacity of n-ZVI to degrade TPH at slightly alkaline pH (as the case of the raw FW with pH 8.6 ± 0.25) may be as result of generation of less competent oxidative species, such as FeO^{2+}, as presented in Eq. (10) [28], and/or precipitation of iron oxy/hydroxides, which is evidenced by the lower concentration of ferrous ions in the FW solution relative to those at low pH conditions (see Section 3.6). Furthermore, degradation experiments at varying pH (5.9 ± 2.6) were carried out to examine the effects of pH on TPH removal from the FW (Fig. 2). As the pH decreases, TPH degradation efficiency increased but decreased with increasing alkalinity. At pH 3, 78.2% reduction of the FW TPH concentration was observed compared to 51% TPH reduction at slightly alkaline pH, after 60 min of reaction. This finding was in agreement with the activity of ZVI investigated at lower pH (4 ± 1) values in oxic conditions [24,36,45] though, the target pollutants in this case were TPH other than those reported. As described in Eq. (11), the production of hydroxyl radicals by ferryl ions may be responsible for the sustained degradation of the FW TPH at alkaline pH condition (pH 8.6) as it increases from 21% after 5 min to about 51% after 60 min at pH 8.6 (Fig. 2a). The rate of degradation of TPH at 2 g/L n-ZVI under oxic condition was best described by the pseudo-second-order kinetic model (Eq. (18)).

$$1/[TPH] - 1/[TPH]_0 = K_{rc}\Delta t \quad (18)$$

where k_{rc} is the reaction rate constant which can be obtained by fitting the data in Eq. (18). As shown in Fig. 2(b), the degradation rate of TPH was accelerated by an approximate factor of 6 and 5, at pH 3 (k_{rc} = 0.00272 min^{-1}), and pH 4 (k_{rc} = 0.00250 min^{-1}), respectively, and by a factor of 3.5 at pH 5 (k_{rc} = 0.00163 min^{-1}), compared to pH of the raw FW at pH 8.6 (k_{rc} = 0.00046 min^{-1}). This clearly demonstrates that reaction pH is notably important for the removal of TPH from FW. The coefficients of determination (r^2) all have values greater than 0.9 when kinetic plots were computed from data points within 15 min of reaction.

To quantify the effect of ROS on the reaction kinetic, stoichiometric amount of H_2O_2 was added to the reaction of 2 g n-ZVI in a liter of raw FW and aerated at 1.5 L/min in parallel with other pH reaction conditions (Fig. 2). Results show that addition of hydrogen peroxide at pH 3 (k_{rc} = 0.0029 min^{-1}), accelerated the degradation of TPH over 6 times, than at pH 8.6, and by a factor of 1, compared to those at the same condition (pH 3) without H_2O_2 addition. This result is in accordance with the findings of Segura et al. [36], where they observed remarkable TOC conversions in Air/ZVI/H_2O_2 system, compared to the system with only Air/ZVI. Moreover, our study show that within 30 min, TPH degradation reached up to 81% in the n-ZVI/O_2/H_2O_2 system at pH 3,

Table 3
index of FW under different treatment conditions (reaction time: 120 min; air flow rate: 1.5 L/min).

Sample no.	n-ZVI, g/L	Condition	BOD_5, mg/L	COD, mg/L	BOD_5/COD	COD/COD_0
1	0	pH 8.6	214.0	2310.0	0.093	1.00
2	2.0	pH 3.0	208.0	1196.5	0.174	0.52
3	2.0	pH 3.0 + H_2O_2*	222.0	1068.5	0.208	0.46
4	2.0	pH 4.0	177.0	1625.5	0.109	0.70

* H_2O_2 was added in stoichiometric amount based on the initial total organic carbon conversion.

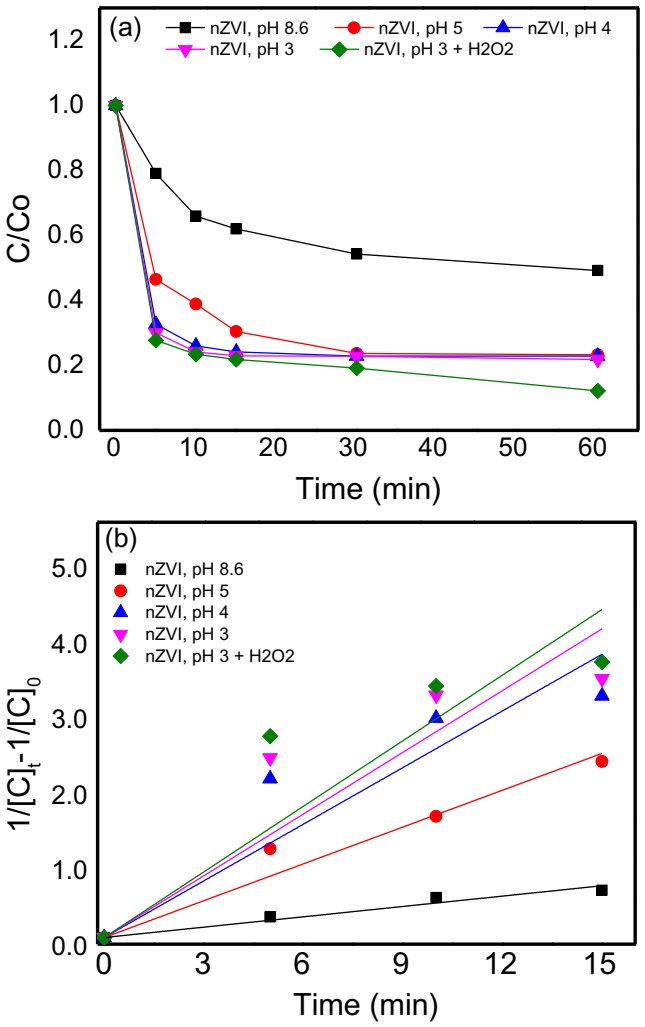

Fig. 2. (a) Effects of pH on the degradation of TPH; (b) kinetic plot of TPH removal from FW at varying pH using n-ZVI initiated oxidation. (Experimental conditions: C_0 = 109.8 mg/L; 2 g/L n-ZVI; air flow rate of 1.5 L/min, 8.5 mM H_2O_2).

which is higher in magnitude compared to the TPH removal efficiency (78%) in the n-ZVI/O_2 system at similar pH value but after 60 min. Hence, this implies that, at shorter reaction time, treatment cost and energy consumption could significantly be reduced when the ZVI/O_2/H_2O_2 system is utilized for the treatment of TPH in FW (see Section 3.9 for more detailed discussion).

3.5. PEGs

3.5.1. Mechanism of PEGs removal from FW

After completion of the reaction involving 2 g/L n-ZVI at pH 4 ± 1 and 8.6 under oxic conditions, PEG-400 removal at different times from the FW were analytically detected in the filtered samples as shown in Fig. 3. Among the eight identified PEG oligomers in the FW, seven of them were more prominent with higher peaks (Fig. S2 of SI), using PEG-400 standard as identifier [40,41]. Accurate mass spectrometry determination using the PEG-400 standard revealed that most of the identified PEGs in the as-received wastewater were significantly reduced or completely removed/-transformed after reaction with the iron nanoparticles within 120 min. Although, PEGs removal by n-ZVI alone in the presence of oxygen was significant (Fig. 3), the highest removal was observed in the reaction supplemented by H_2O_2. In a study conducted by Fukatsu and Kokot [50], degradation of Poly(ethylene

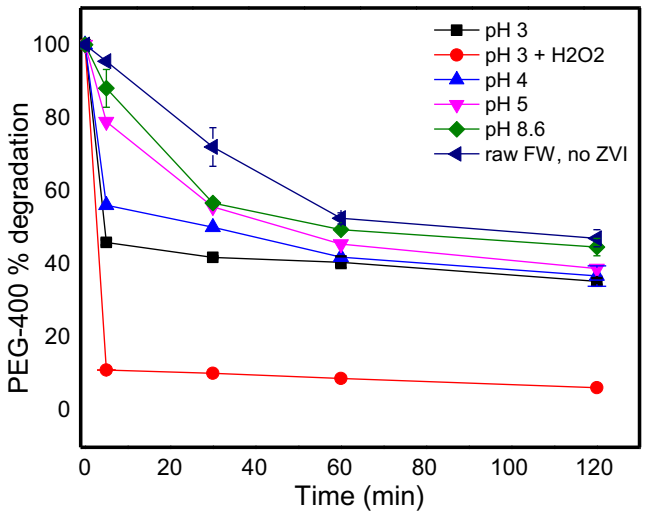

Fig. 3. Degradation efficiency of PEG-400 in FW by n-ZVI at different times and varying pH. (Experimental conditions: 2 g/L n-ZVI; air flow rate of 1.5 L/min).

oxide) (PEO) following increase of H_2O_2 concentration resulted in no obvious viscosity change (a measure of PEO degradation). However, the presence of Cu^{2+} ions in a Cu^{2+}/H_2O_2/PEO electrolytic system brought about the increased generation of hydroxyl radicals which led to a significant reduction in the viscosity of PEO and thus, showing the importance of catalyst addition to promoting the degradation of PEO. The action of n-ZVI in FW under oxic condition follows similar reaction mechanism.

In the reaction at pH 3 without H_2O_2 addition, the maximum degradation efficiency of the FW PEGs was nearly 64.6% after 120 min. Chen et al. [27] described the degradation mechanism of Orange II and its hydroquinone-like intermediates to be linked with the generation of non-aromatic intermediates, such as, oxalate, malonic acid and acetic acid, which notably inhibited the production of Fe^{2+} for catalysis of H_2O_2. Similarly, non-aromatic compounds like PEGs could suppress the reaction between Fe^{3+} and H_2O_2 by preferably chelating with Ferric ions as also described in Eq. (9). This action prevents the recycle of Fe^{3+} to Fe^{2+} which is important for radical generation, and thus, the reduction in

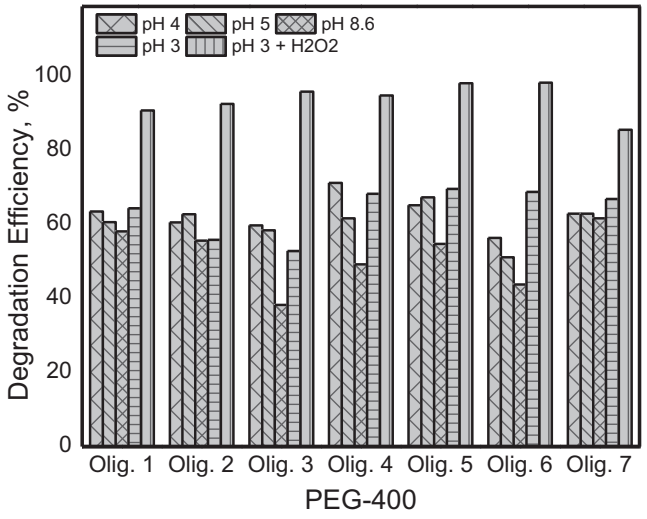

Fig. 4. Effect of various n-ZVI treatment systems on degradation of PEG-400 oligomers in FW at pH 3 (with and without H_2O_2), 4, 5 and 8.6 (Experimental conditions: 2 g/L n-ZVI; air flow rate of 1.5 L/min).

degradation rate of the FW PEGs at all pH values including pH 3 as shown in Fig. 4. However, within 5 min of reaction in the n-ZVI/O_2/H_2O_2 system, most of the FW PEGs component was reduced from 100% to 11.1% at 60 min, and to 6.3% after 120 min at pH 3, indicating the role of increased hydroxyl radical ($HO^{\cdot}$) production through Fenton reaction (see Eqs. (5–7)), which consequently led to the degradation of the PEGs in the FW (Fig. 4). The high surface reactivity of n-ZVI in the presence of oxidative species, such as H_2O_2, may equally have resulted in the fast degradation kinetics observed for PEGs in the FW, as the scavenging effects of Fe^{2+} is highest in the presence of oxidants [26]. Besides, production of Fe^{2+} increased until 5 min before gradually declining (as discussed in Section 3.6). This implies that few minutes into the reaction, the scavenging effect of Fe^{2+} was the dominant mechanism leading to degradation of the FW PEGs. However, with time, the concentration of Fe^{3+} increased and thus, the residual H_2O_2 instead of being catalyzed to generate radicals, formed complex with ferric ions leading to the reduction in the degradation efficiency of the all the systems including those supplemented with H_2O_2 during the remaining reaction time after the initial 5 min (Fig. 3).

In the raw FW, oligomers 5 and 7 had the highest concentration 2.72 ± 1.0 and 3.5 ± 1.1 mg/L, respectively. From the results, degradation efficiencies of each oligomer vary within the PEGs and the treatment systems. Both n-ZVI/O_2 and n-ZVI/O_2/H_2O_2 systems effectively degrade Oligomer 5 up to 69.6% and 98.2% at pH 3, respectively (Fig. 4). Oligomer 7 was the least degraded in the n-ZVI/O_2/H_2O_2 system probably due to concentration of the repeating oligomer unit. However, while Oligomer 3 degradation in the n-ZVI/O_2 system appeared sluggish at all tested pH conditions (Fig. 4), it was quickly degraded in the n-ZVI/O_2/H_2O_2 system. The efficiency of the oligomers degradation at pH 4 and 5 were comparable, but slightly reduced at pH 8.5. This further confirms the oxidative effect of hydrogen peroxide to enhance degradation of the FW PEG oligomers, as similarly observed by Segura et al. [30], in the treatment of pharmaceutical wastewater augmented with H_2O_2.

3.5.2. Proposed PEGs degradation pathway by n-ZVI

We proposed that the mechanism of PEGs degradation by n-ZVI followed the release of $HO^{\cdot}$ which interact with PEGs compounds to produce internally generated PEG radical, and further dissociates to form aldehyde and smaller units of vinyl and alkyl ethers (Fig. 5). However, to experimentally confirm the proposed PEGs degradation pathway in FW, the seven most informative and abundant molecular ions for pure PEG 400 in MRM mode were selected at m/z 283.1 (Oligomer 1), 327.1 (Oligomer 2), 388.2 (Oligomer 3), 432.4 (Oligomer 4), 476.3 (Oligomer 5), 520.2 (Oligomer 6), 564.3 (Oligomer 7), using declustering potentials of 86 to 71 V, respectively. The chromatogram representing the seven oligomers is presented in Fig. S3. of SI. Of the masses corresponding to the in-source fragmentation of the various oligomers, the fragment ions at m/z 45.2, 89.20 and 133.20 were identified as product ions for the PEG 400 oligomers [41]. Representative parent and product ions from the pure PEG are presented in Fig. S4. of SI. Three of the peaks from the PEG-400 product ions possess similar masses to the proposed degradation products, and are as follows: m/z at 45.2 corresponds to the molecular weight (MW) of dimethyl ethyl (MW: 46.07 g/mol), m/z at 89.2 corresponds to MW of ethylene glycol vinyl ether (MW: 88.11), and m/z at 133.20 mass corresponds to diethylene glycol monomethyl ether (MW: 134.7) and di(ethylene glycol) vinyl ether (MW: 132.16), respectively. Moreover, these degradation products were comparable to those found by Lattimer [51] during the pyrolysis of PEGs at 150 °C under inert atmosphere.

3.6. Influence of Fe ions and DO on TPH and PEG removal

The influence of Fe (II) and (III) ions concentrations on degradation rate of the FW organic complex (including TPH and PEGs) was monitored during the whole experiment (Fig. 6). As shown in Fig. 6 (a), the dissolution concentration of Fe^{2+} was highest at pH 3 (2.32 mg/L) relative to pH 4 (1.29 mg/l) and pH 8.6 (0.15 mg/L) on addition of n-ZVI to the fracking wastewater. Dissolution of n-ZVI at lower pH is a well-known process in the literature [32,36,45,49]. However, after 5 min of reaction, the concentration of Fe^{2+} gradually decline probably due to increase of pH, and reached equilibrium after 30 min. As earlier described, Fe^{2+} is inextricably linked with generation of hydroxyl radicals, and this was confirmed by the rate of degradation of the FW TPH and PEGs (where almost 55 –70% of the pollutants were removed within 5 min). Unlike the reduction of Fe^{2+} concentration to nearly zero values at pH 4 and 8.6, it persisted at moderate concentrations of ca. 1.2 mg/L in the aqueous solution after 120 min at pH 3. This could be as a result of Fe^{2+} regeneration as described in Eq. (8). In addition, due to the complexity of the fracking wastewater, organic radicals may be generated as described in equation Eqs. (6) and (7), which subsequently could act as Fe^{3+} reductant, thereby maintaining the concentration of Fe^{2+} at pH 3 as shown in Fig. 6(a).

Moreover, the Fe^{2+} produced at this point might react with in-situ generated H_2O_2 to produce weaker oxidative species of FeO^{2+}- due to increased pH condition. Interestingly, in the control sample (initial FW at pH 8.6, n-ZVI = 0), Fe^{2+} concentration increased from the initial 54 μg/L to 156 μg/L on sparging with air. The increased concentration of Fe^{2+} (possibly as a result of reduction of Fe^{3+}) may have provoked its reaction with oxygen to produce intermediates (e.g. hydrogen peroxides) and reactive oxygen species (including hydroxyl radicals, hydroperoxyl radicals and ferryl ions) in aqueous solution for the degradation of the organics as shown in Eqs. (5–8,10,11). Similarly, the decrease of Fe^{3+} concentration from the initial 598 μg/L to 322 μg/L simultaneously occurred (Fig. 6b). This may be due to generation of internal organic radicals ($R^{\cdot}$) which could reduce Fe^{3+} to Fe^{2+} as described in Eq. (8) [52], or could react with hydrogen peroxides to produce hydroperoxyl radicals Eq. (4) [52]. These radicals (ferryl ions and hydroperoxyl) are weaker oxidants compared to hydroxyl radicals due to their slow rate of generation and their contaminant removal pathway [45]. As shown in Fig. 6(c), the total Fe increased at all tested pH except at pH 8.6 (initial pH of FW), which agrees well with the release of Fe^{2+} and Fe^{3+} as described above. A total Fe ion steady-state concentration of 2.4 mg/L and 1.3 mg/L was reached after 30 min and 60 min, respectively at pH 3 and 4. However, the total Fe ion concentration at pH 8.6 (with and without n-ZVI) was nearly zero after 120 min of reaction. This may be due to suppression of n-ZVI dissolution at higher pH as also reported by other authors [25,53].

DO is quite a significant factor for the removal of the FW organic complex. Therefore, to control the DO at a steady-state, a constant air-flow rate of 1.5 L/min was adapted in all reactors and DO concentration in the reactors were measure at determined time intervals throughout the experiment. The DO concentration profiles at pH 3, 4, & 8.6 are shown in Fig. S5. of SI. The initial rapid decrease of DO from saturation concentrations of 7.9, 7.1 and 7.92 mg/L to 5.8, 5.3, and 7.8 mg/l, respectively at pH 3, 4 and 8.6 within 5 min reaction time suggest that DO consumption by Fe^{2+} (released from the n-ZVI surface) was an important step for the degradation of the FW organics as described in Eq. (3). The high DO consumption rate could also be due to formation of oxide/hydroxide layers of Fe, which occurred very quickly enough to evidence the shortage of oxygen supplied by air sparging (Eqs. (12–6)). Feitz et al. [54] found that during the oxidative degradation of molinate, the DO concentration decreased drastically on addition of n-ZVI, but

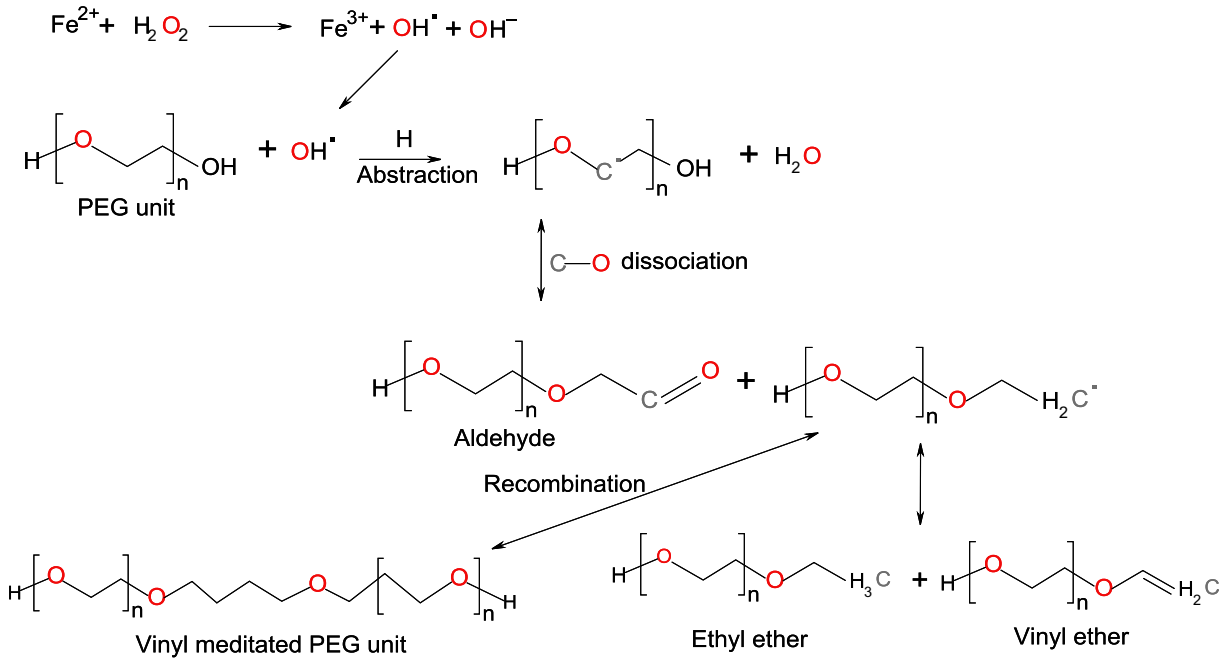

Fig. 5. Proposed PEGs degradation pathway in fracking wastewater by n-ZVI initiated hydroxyl radical production.

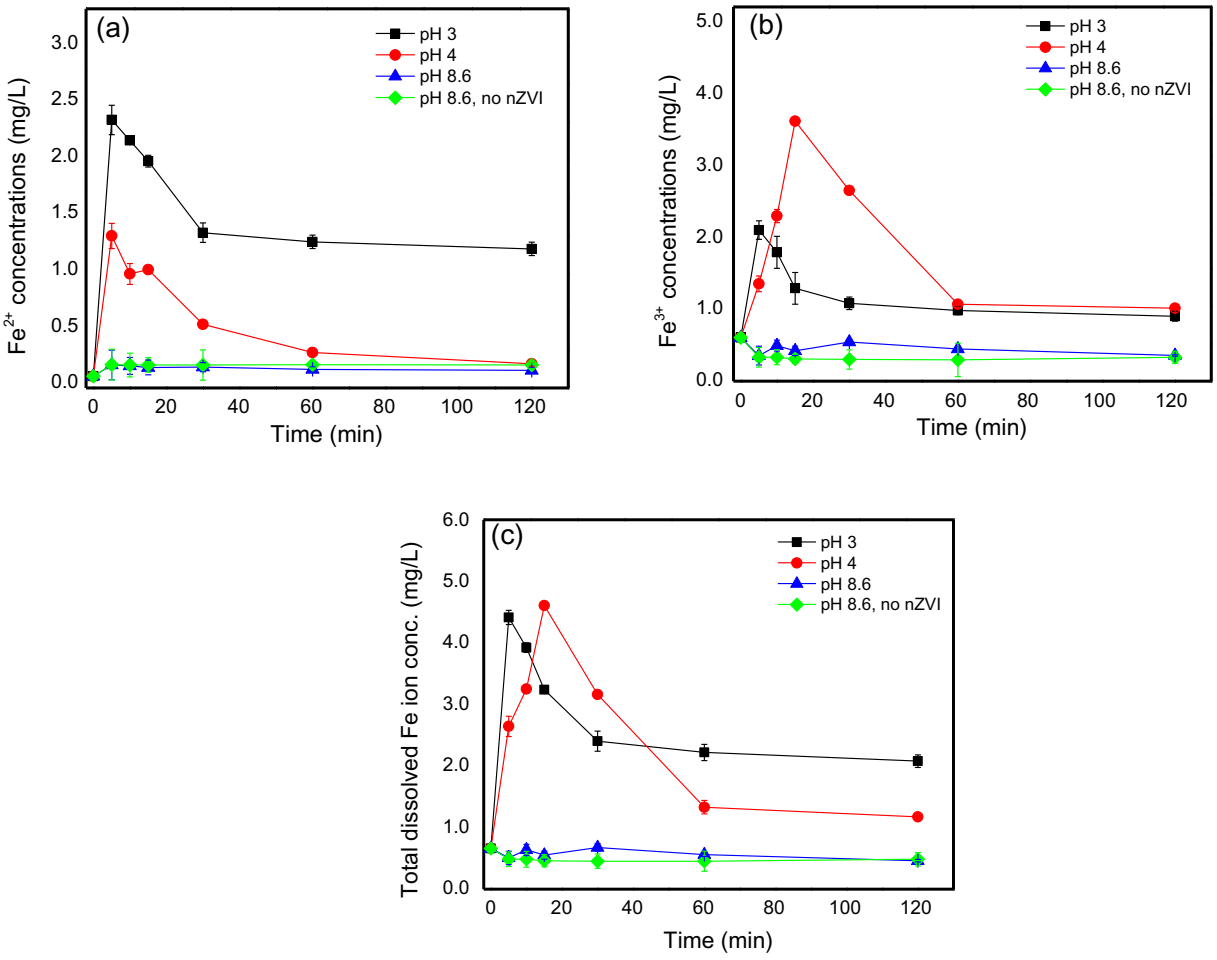

Fig. 6. Effect of initial start-up pH on n-ZVI dissolution during fracking wastewater treatment (a) Ferrous ion elution concentration (b) Ferric ion elution concentration, and (c) total dissolve Fe ion concentration (Experimental conditions: 2 g/L n-ZVI; air flow rate of 1.5 L/min).

gradually return to the near saturation condition after 200 min of reaction. The gradual recovery of DO in this study was quite similar to theirs, but was achieved rather earlier at around 60 min, which is relatively slower than those reported by Harada et al. [45] occurring at less than 6 min. Further to the study conducted by Harada et al. [45], the highest concentration of n-ZVI utilized in their was ca. 0.076 g/L, whereas in this study about 2 g/L n-ZVI was utilized for degradation of the fracking wastewater. Exposure of n-ZVI surface to oxygen and H_2O molecules could increase the passivation of the exposed n-ZVI surface (by formation of oxides/hydroxides of Fe) with accompanying decrease in DO consumption rate. This could complementarily depress the elution of $Fe^{2+}$and subsequently inhibit the formation of H_2O_2 as the passivation layer pervade the entire n-ZVI surface. Hence, the specific surface area of n-ZVI may be responsible for the dissimilar oxygen consumption rate reported in this study relative to the aforementioned study, which invariably may also affect the degradation kinetics of organic pollutants (although, the wastewater composition/type are also important).

The DO consumption rate and the release of Fe^{2+} follows a similar trend as observed in the degradation of the FW TPH and PEGs, which mostly occurred within a reaction time of about 5 min. At pH 8.6, only a few amount of DO was used (under saturated concentration) probably due to lower release of Fe^{2+} at alkaline pH. However, in low DO or anoxic conditions, generation of reactive oxygen species including hydroxyl radicals were not observable despite release of Fe^{2+} in the anoxic aqueous solution [45]. This makes clear the role of oxygen in the generation of ROS for organic degradation.

3.7. FTIR measurement of sorbed FW organics by n-ZVI

Sorption of pollutants on n-ZVI surface played an important role in the removal of the FW organics. Spectra of Fresh (control) and spent n-ZVI samples subjected to Fourier transform infrared (FTIR) measurement were collected to verify the occurrence of organic sorption on the n-ZVI samples. Results show that unlike the fresh n-ZVI (which showed the presence of Fe oxides peak at 603 cm^{-1}), spectrum of the spent n-ZVI sample confirmed the presence of reduced or oxidized forms of the FW TPH and PEGs as shown in Fig. 7. Major IR stretching vibrations at 3397, 2963, 2925, 2853, 1261, 1101, 1025, 802, and 458 cm^{-1} which likely corresponds to –OH, asymmetric (first two peaks) and symmetric (last of the three peaks) straight chain stretching vibration of C–H alkanes (–C–CH_2–C), symmetric bending of Si bonded –CH_3, symmetric straight chain and stretching vibration of saturated C–O ethers (C–O–C), and organic P bonded O–CH_3 symmetric straight chain were found respectively [55–57]. Most of the groups identified in the FTIR analysis were similar to those detected in the degradation products of TPH (not shown) and PEGs (e.g. ether groups), which also suggest that degradation of the organics had occurred before adsorption took place. Furthermore, as shown in the TOC experiments, no more than 22% reduction of total organic carbon in the treated FW was observed, which means that only a small fraction of the organics was mineralized or removed by adsorption (which may partly be due to limited surface area for sorption on n-ZVI). Unlike TOC reduction (22%), TPH (87.8%) and PEGs (93.7%) reductions suggest that their removal pathway by n-ZVI is likely due to oxidative degradation rather than adsorption.

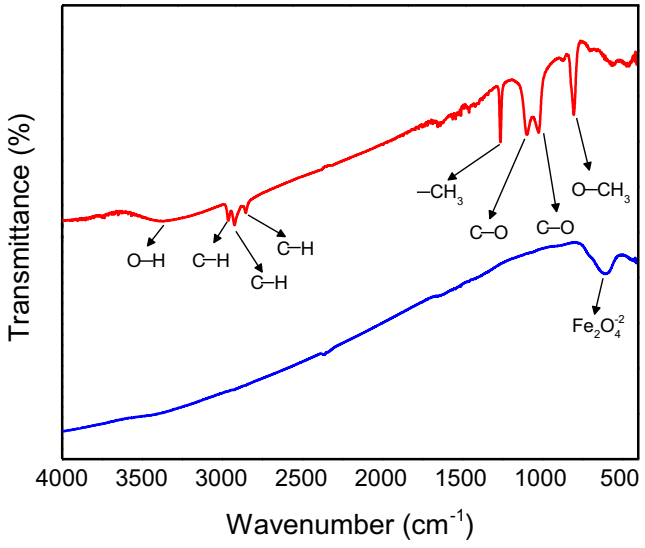

Fig. 7. FTIR spectra of spent n-ZVI (in red line) and fresh n-ZVI (in blue line). (For interpretation of the references to colour in this figure legend, the reader is referred to the web version of this article.)

3.8. Metals and non-metals recovery from FW

Samples of spent n-ZVI mixed with solid suspensions from the FW were retrieved from the treatment reactors and analyzed using XRD and XRF techniques. The XRD patterns of the pristine and spent n-ZVI are shown in Fig. 8. The XRD results reveal that the main composition of the pristine n-ZVI is metallic iron (Fe^0) at peak position 2θ of 44.6° (Fig. 8). However, after reaction with the fracking solution in oxic condition, the intensity of the Fe^0 peak was sharply reduced, owing to the formation of oxide/hydroxides on rapid oxidation of the Fe^0 by oxygen and potential oxidants such as hydrogen peroxide (Fig. 8). The Fe-oxy/hydroxides formed (including magnetite/maghemite, iron oxide, hematite, and hematite (proto)/goethite) play vital role in the removal of organics, metals and heavy metals through the process of electrostatic and chemical adsorption, precipitation with hydroxides ions and co-precipitation, as also observed in previous works [19–21].

To quantify the chemical elements removal capacity of n-ZVI, XRF analysis was performed, and results revealed that most of the metals and non-metals (including Sr, Mg, Na, Al, Ca, K, P, Cl, S) with concentrations >50 μg/g in the initial FW could be detected by the spectroscopic method (Fig. 9). The recovered concentrations of metals and non-metals on the n-ZVI surface were relatively higher for n-ZVI/O_2/H_2O_2 system, than for the n-ZVI/O_2 system,

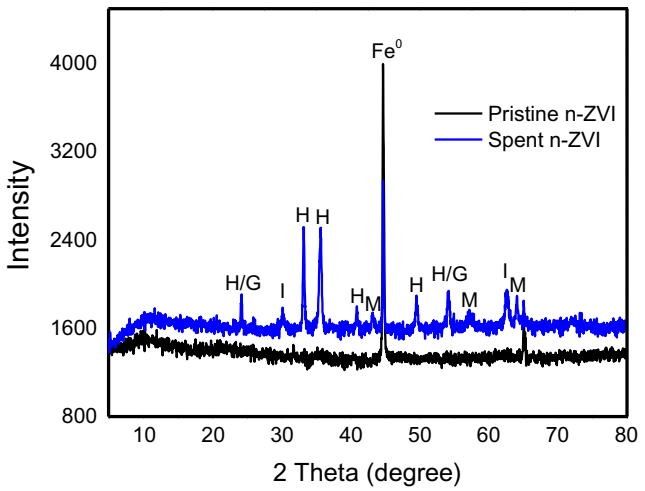

Fig. 8. XRD patterns of the pristine n-ZVI and spent n-ZVI after reaction with fracking wastewater (Peaks corresponds to hematite (proto)/goethite (H/G), iron oxide (Fe_2O_3) (I), hematite (Fe_2O_3) (H), magnetite (Fe_3O_4)/maghemite (γ – Fe_2O_3) (M), and n-ZVI (Fe^0).

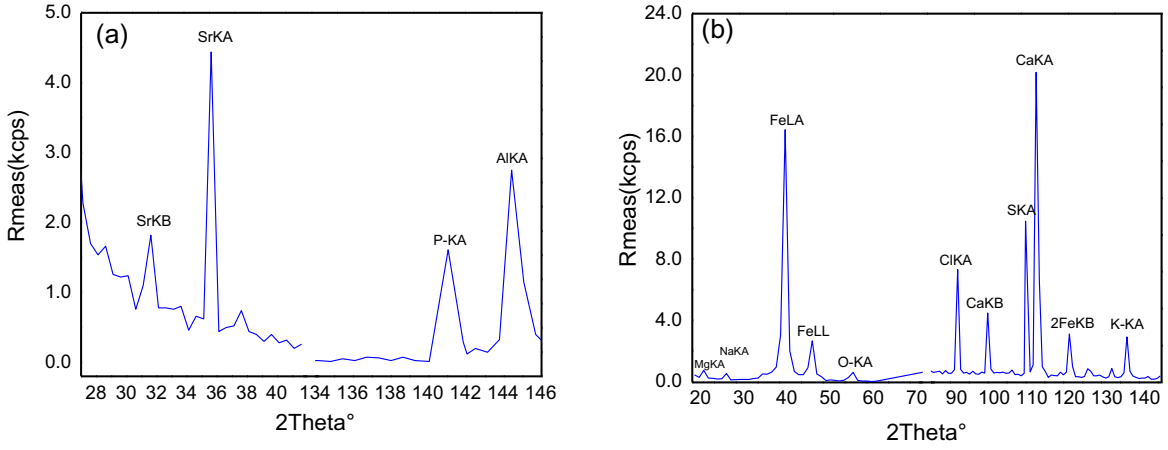

Fig. 9. XRF probe of spent n-ZVI revealing the recovery of a) Sr, P, Al, b) Mg, Na, Cl, S, Ca, and K from the fracking wastewater.

as shown in Fig. 10. This is likely as a result of the rigorous corrosion of the n-ZVI surface in the presence of the oxidant, producing oxides and Fe-oxy/hydroxides (as confirmed by the XRD analysis) involved in the sorption of the metals and non-metals from the FW. This observation is in agreement with the results presented by Guo et al. [20]. Interestingly, among the sorbed elements on the n-ZVI surface is chlorine (Cl) as revealed by XRF spectroscopy (Fig. 9b). The presence of halocarbons in FW has been associated with the reuse of treated wastewater retrieve from facilities that employs chlorine containing oxidants for bacteria removal [33]. Such chlorinated waters are believed to react with native materials within the fracked formation to form halocarbons which constitutes potential health hazards [58]. Therefore, the use of n-ZVI for the treatment of fracking wastewater could be a viable treatment option to eliminate halocarbons occurrence in the reuse of fracking wastewater.

3.9. Cost evaluation

In most available literatures, cost assessment for wastewater treatment is often based on electrical energy consumption [59,60], except for few that takes into account reagent costs [46,48]. In contrast, in application such as Fenton-like processes, the use of n-ZVI may account for most of the operating cost compared to the cost of electricity used up in the treatment process. Besides, the computation of treatment cost based on specific removal target (e.g. TPH or PEGs) will be inequitable considering the complex nature of real industrial wastewater matrix (like FW). Cost indications stemming from such calculations may not totally reflect the treatment efficiency of the Fenton/Fenton-like system used, as it precludes the removal cost for other organic and inorganic components of the wastewater. Moreover, use of TOC and COD removal index for cost calculation may be more significant, but again, this undermines the pretreatment effect of n-ZVI, which aids the degradation of recalcitrant or refractory components of the wastewater (in this case, FW), making them easily accessible to micro-organisms for complete mineralization [61]. This synergistic approach has also been recently reported by Huang et al. [62]. Nonetheless, a cost estimate based on TPH and PEGs degradation in the FW is presented in Table S2. The operation cost evaluated in terms of reagent costs [n-ZVI (99.9% metal basis): \$80–\$150/kg depending on the quantity purchased and size of the nanomaterial; H_2O_2 (30%): \$3.48/kg], and electricity cost (\$0.10/kWh) are presented in Table 4. The calculation of the electrical energy cost per order (EE/O) was modified after Bolton et al. [63] and is shown in Eq. (19).

$$EEM/O(kWh/m^{-3}) = [(P_a + P_s) \times t]/V \quad (19)$$

where P_a and P_s represent the air pump and stirrer energy inputs, respectively, t is the time in 'h' to achieve TPH and PEGs removal, and V is the volume of FW treated in m^{-3}.

It can be observed from Table S2, that the cost of treatment for TPH and PEGs using n-ZVI/O_2/H_2O_2 system is relatively cheaper than that of n-ZVI/O_2 system during treatment of FW. Whereas the operating cost per targets removal (TPH and PEGs) within 5 min of treatment with the n-ZVI/O_2 was \$100.22, it was only \$78.57 at the same time required for the n-ZVI/O_2/H_2O_2 treatment

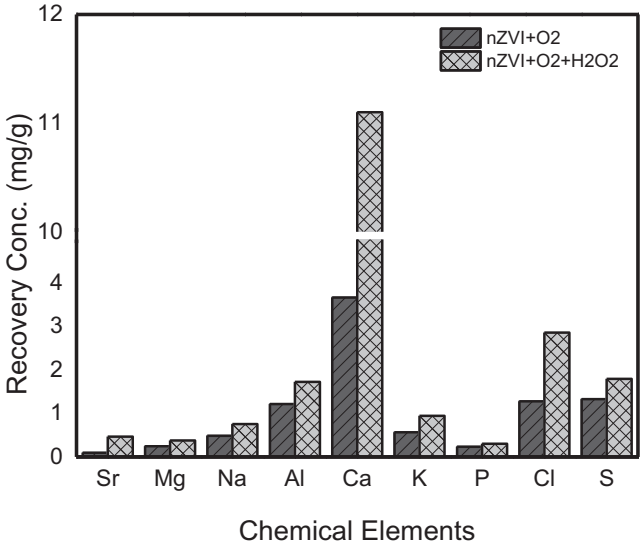

Fig. 10. Metals and non metals recovery from fracking wastewater by n-ZVI at pH 3 after 1 h at different reaction conditions (Experimental conditions: 2 g/L n-ZVI; air flow rate of 1.5 L/min, 85 mM H_2O_2).

Table 4
Operating cost value input.

Process parameters	Value
n-ZVI	2 kg/m^3
H_2O_2	2.9 kg (H_2O_2 30% weight basis)/m^3
Operating reactor volume	10^{-3} m^3
Reaction time	0–2 h
Air pump energy used	0.024 kWh
Jar stirrer energy used	0.03 kWh

system. The additional cost of H_2O_2 oxidant proved negligible as moderate amounts of the oxidant could effectively enhance the degradation of the FW major organic components without imparting the total operating cost. Compared to other works involving Fenton reaction [60,64], reagents cost associated with pretreatment of FW using n-ZVI appears higher ($200/m^{-3}), which is likely due to the prevailing market price of n-ZVI, the use of n-ZVI primary formulation materials (like $FeSO_4$ H_2O) in estimation of reagent cost in the mentioned literatures, and the difference in wastewater matrix. Moreover, the degradation/removal of TPH (88%) and PEGs (91%) from FW show satisfactory results after one hour of treatment and may even be more promising, as n-ZVI can be regenerated (under high temperature and hydrogen streaming) and reused while exerting similar degradation characteristics as its freshly prepared equivalent [49].

4. Conclusions

Channeling the reuse of fracking wastewater is essentially a suited alternative both for environment protection and release of stress on the limited water resources. In this study, we characterized the fracking wastewater from Yanchang Formation, southeastern Ordos Basin and demonstrated the effectiveness of n-ZVI initiated oxidation/adsorption to achieve reuse of the fracking wastewater through simultaneous degradation of complex organics (including TPH and PEGs), and recovery of potential chemical elements, respectively. The major findings are as follows:

1) Unlike TOC (22%), TPH (87.8%) and PEGs (93.7%) reductions suggest that their removal pathway by n-ZVI is likely due to oxidative degradation rather than adsorption, and biodegradability of the fracking wastewater was significantly enhanced by 55%.
2) Iron dissolution and oxygen consumption rates play significant roles in the production of reactive oxidation species which in turn influence the degradation/removal rates of the FW organic components.
3) Degradation of PEGs by n-ZVI was greatly influenced by the reaction pH and the presence of oxidants. It is proposed that PEGs degradation pathway by n-ZVI follows the release of $HO^{\cdot}$ in both n-ZVI/O_2 and n-ZVI/O_2/H_2O_2 aqueous systems, respectively to provoke the production of PEG internal radicals following the scission of the C–O bond and thus, producing decomposition products of vinyl and ethyl ethers as confirmed by LC-MS/MS.
4) Spectroscopic evidence shows the removal of chlorine – a precursor to halocarbon formation in fracked wells, and recovery of other potential chemical elements by n-ZVI corrosion products formed during reaction with the fracking wastewater.
5) TPH degradation reached up to 81% in the n-ZVI/O_2/H_2O_2 system at pH 3 within 30 min, which is higher than the TPH removal efficiency (78%) in the n-ZVI/O_2 system at similar pH value but after 60 min. Hence, this implies that, at shorter reaction time, treatment cost and energy consumption could significantly be reduced when the ZVI/O_2/H_2O_2 system is utilized for the treatment of TPH in fracking wastewater.

Acknowledgements

This work was supported by funds from the Key Project of International Cooperation, Bureau of International Co-operation, CAS, and the Chinese Academy of Sciences-The World Academy of Sciences (CAS-TWAS) president's fellowship program for developing countries. K.S. Zhang thanks Royal Academy of Engineering, UK for the research exchange with China/India scheme. We acknowledge Mr. Lifeng Lin and MS. Chi Qiaoqiao for their help with LC–MS/MS and ICP-MS analysis, and Ms. Jiani Wang for technical support with XRF analysis. Ms. Gloria Oyagha technical assistance is also acknowledged.

Appendix A. Supplementary data

Supplementary data associated with this article can be found, in the online version, at http://dx.doi.org/10.1016/j.cej.2017.07.030.

References

[1] EIA, The Annual Energy Outlook, April 2015, Tech. rept. U.S. Department of Energy, Energy Information Administration, 2015.
[2] K.B. Gregory, R.D. Vidic, D.A. Dzombak, Water management challenges associated with the production of shale gas by hydraulic fracturing, Elements 7 (2011) 181–186.
[3] K.J. Bibby, S.L. Brantley, D.D. Reible, K.G. Linden, P.J. Mouser, K.B. Gregory, B.R. Ellis, R.D. Vidic, Suggested reporting parameters for investigations of wastewater from unconventional shale gas extraction, Environ. Sci. Technol. 47 (2013) 13220–13221.
[4] I. Ferrer, E.M. Thurman, Chemical constituents and analytical approaches for hydraulic fracturing waters, Trends Environ. Anal. Chem. 5 (2015) 18–25.
[5] W.T. Stringfellow, J.K. Domen, M.K. Camarillo, W.L. Sandelin, S. Borglin, Physical, chemical, and biological characteristics of compounds used in hydraulic fracturing, J. Hazard. Mater. 275 (2014) 37–54.
[6] B. Akyon, E. Stachler, N. Wei, K. Bibby, Microbial mats as a biological treatment approach for saline wastewaters: the case of produced water from hydraulic fracturing, Environ. Sci. Technol. 49 (2015) 6172–6180.
[7] Y. Lester, I. Ferrer, E.M. Thurman, K.A. Sitterley, J.A. Korak, G. Aiken, K.G. Linden, Characterization of hydraulic fracturing flowback water in Colorado: implications for water treatment, Sci. Total Environ. 512–513 (2015) 637–644.
[8] K. Kano, M. Horikawa, T. Utsunomiya, M. Tati, K. Satoh, S. Yamaguchi, Lung cancer mortality among a cohort of male chromate pigment workers in Japan, Int. J. Epidemiol. 22 (1993) 16–22.
[9] J.S. Rosenblum, K.A. Sitterley, E.M. Thurman, I. Ferrer, K.G. Linden, Hydraulic fracturing wastewater treatment by coagulation-adsorption for removal of organic compounds and turbidity, J. Environ. Chem. Eng. 4 (2016) 1978–1984.
[10] Y. Lester, T. Yacob, I. Morrissey, K.G. Linden, Can we treat hydraulic fracturing flowback with a conventional biological process? The case of guar gum, Environ. Sci. Technol. Lett. 1 (2014) 133–136.
[11] B. Xiong, A.L. Zydney, M. Kumar, Fouling of microfiltration membranes by flowback and produced waters from the Marcellus shale gas play, Water Res. 99 (2016) 162–170.
[12] J.M. Estrada, R. Bhamidimarri, A review of the issues and treatment options for wastewater from shale gas extraction by hydraulic fracturing, Fuel 182 (2016) 292–303.
[13] J. Dai, M. Xu, J. Chen, X. Yang, Z. Ke, PCDD/F PAH and heavy metals in the sewage sludge from six wastewater treatment plants in Beijing, China, Chemosphere 66 (2007) 353–361.
[14] J. Xiao, B. Gao, Q. Yue, Y. Gao, Q. Li, Removal of trihalomethanes from reclaimed-water by original and modified nanoscale zero-valent iron: Characterization, kinetics and mechanism, Chem. Eng. J. 262 (2015) 1226–1236.
[15] L. Zhao, Y. Ji, D. Kong, J. Lu, Q. Zhou, X. Yin, Simultaneous removal of bisphenol A and phosphate in zero-valent iron activated persulfate oxidation process, Chem. Eng. J. 303 (2016) 458–466.
[16] R.A. Crane, M. Dickinson, T.B. Scott, Nanoscale zero-valent iron particles for the remediation of plutonium and uranium contaminated solutions, Chem. Eng. J. 262 (2015) 319–325.
[17] Y. Sun, S.S. Chen, D.C. Tsang, N.J. Graham, Y.S. Ok, Y. Feng, X.D. Li, Zero-valent iron for the abatement of arsenate and selenate from flowback water of hydraulic fracturing, Chemosphere 167 (2016) 163–170.
[18] O.K. Abass, T. Ma, S. Kong, Z. Wang, M.T. Mpinda, A novel MD-ZVI integrated approach for high arsenic groundwater decontamination and effluent immobilization, Process Saf. Environ. Prot. 102 (2016) 190–203.
[19] T.B. Scott, I.C. Popescu, R.A. Crane, C. Noubactep, Nano-scale metallic iron for the treatment of solutions containing multiple inorganic contaminants, J. Hazard. Mater. 186 (2011) 280–287.
[20] X. Guo, Z. Yang, H. Dong, X. Guan, Q. Ren, X. Lv, X. Jin, Simple combination of oxidants with zero-valent-iron (ZVI) achieved very rapid and highly efficient removal of heavy metals from water, Water Res. 88 (2016) 671–680.
[21] C. Noubactep, Metallic iron for environmental remediation: a review of reviews, Water Res. 85 (2015) 114–123.
[22] S. Li, W. Wang, F. Liang, W.X. Zhang, Heavy metal removal using nanoscale zero-valent iron (nZVI): theory and application, J. Hazard. Mater. 322 (2017) 163–171.
[23] O. Špalek, J. Balej, I. Paseka, Kinetics of the decomposition of hydrogen peroxide in alkaline solutions, J. Chem. Soc., Faraday Trans. 1: Phys. Chem. Condensed Phases 78 (1982) 2349.

[24] Y.W. Kang, K.-Y. Hwang, Effects of reaction conditions on the oxidation efficiency in the Fenton process, Water Res. 34 (2000) 2786–2790.
[25] C.R. Keenan, D.L. Sedlak, Factors Affecting the yield of oxidants from the reaction of nanoparticulate zero-valent iron and oxygen, Environ. Sci. Technol. 42 (2008) 1262–1267.
[26] H. Lee, H.J. Lee, H.E. Kim, J. Kweon, B.D. Lee, C. Lee, Oxidant production from corrosion of nano- and microparticulate zero-valent iron in the presence of oxygen: a comparative study, J. Hazard. Mater. 265 (2014) 201–207.
[27] F. Chen, Y. Li, L. Guo, J. Zhang, Strategies comparison of eliminating the passivation of non-aromatic intermediates in degradation of Orange II by Fe3+/H2O2, J. Hazard. Mater. 169 (2009) 711–718.
[28] S.Y. Pang, J. Jiang, J. Ma, Oxidation of sulfoxides and arsenic(III) in corrosion of nanoscale zero valent iron by oxygen: evidence against ferryl ions (Fe(IV)) as active intermediates in Fenton reaction, Environ. Sci. Technol. 45 (2011) 307–312.
[29] S. Zečević, D.M. Dražić, S. Gojković, Oxygen reduction on iron—IV The reduction of hydrogen peroxide as the intermediate in oxygen reduction reaction in alkaline solutions, Electrochim. Acta 36 (1991) 5–14.
[30] S.H. Bossmann, E. Oliveros, S. Göb, S. Siegwart, E.P. Dahlen, L. Payawan, M. Straub, M. Wörner, A.M. Braun, New evidence against hydroxyl radicals as reactive intermediates in the thermal and photochemically enhanced fenton reactions, J. Phys. Chem. A 102 (1998) 5542–5550.
[31] C. Canton, S. Esplugas, J. Casado, Mineralization of phenol in aqueous solution by ozonation using iron or copper salts and light, Appl. Catal. B 43 (2003) 139–149.
[32] F. Fu, D.D. Dionysiou, H. Liu, The use of zero-valent iron for groundwater remediation and wastewater treatment: a review, J. Hazard. Mater. 267 (2014) 194–205.
[33] S.J. Maguire-Boyle, A.R. Barron, Organic compounds in produced waters from shale gas wells, Environ. Sci. Process. Impacts 16 (2014) 2237–2248.
[34] E.M. Thurman, I. Ferrer, J. Blotevogel, T. Borch, Analysis of hydraulic fracturing flowback and produced waters using accurate mass: identification of ethoxylated surfactants, Anal. Chem. 86 (2014) 9653–9661.
[35] S.E. Mylon, Q. Sun, T.D. Waite, Process optimization in use of zero valent iron nanoparticles for oxidative transformations, Chemosphere 81 (2010) 127–131.
[36] Y. Segura, F. Martínez, J.A. Melero, J.L.G. Fierro, Zero valent iron (ZVI) mediated Fenton degradation of industrial wastewater: Treatment performance and characterization of final composites, Chem. Eng. J. 269 (2015) 298–305.
[37] X. Tang, J. Zhang, X. Wang, B. Yu, W. Ding, J. Xiong, Y. Yang, L. Wang, C. Yang, Shale characteristics in the southeastern Ordos Basin, China: Implications for hydrocarbon accumulation conditions and the potential of continental shales, Int. J. Coal Geol. 128–129 (2014) 32–46.
[38] J.E. Amonette, Improvements to the quantitative assay of nonrefractory minerals for Fe(II) and total Fe using 1,10-phenanthroline, Clays Clay Miner. 46 (1998) 51–62.
[39] C.M. Reddy, J.G. Quinn, GC–MS analysis of total petroleum hydrocarbons and polycyclic aromatic hydrocarbons in seawater samples after the North Cape oil spill, Mar. Pollut. Bull. 38 (1999) 126–135.
[40] M. Lichtenegger, M. Rychlik, Development of a stable isotope dilution LC-MS assay for the quantitation of multiple polyethylene glycol (PEG) homologues to be used in permeability studies, J. Chromatogr. B Anal. Technol. Biomed. Life Sci. 1001 (2015) 182–190.
[41] V. Vijaya Bhaskar, A. Middha, S. Tiwari, S. Shivakumar, Liquid chromatography/tandem mass spectrometry method for quantitative estimation of polyethylene glycol 400 and its applications, J. Chromatogr. B Anal. Technol. Biomed. Life Sci. 926 (2013) 68–76.
[42] U.S.E.P.A. USEPA, National Primary Drinking Water Regulations, http://www.epa.gov/safewater/consumer/pdf/mcl.pdf., 2009.
[43] J. Parnell, C. Brolly, S. Spinks, S. Bowden, Selenium enrichment in carboniferous shales, Britain and Ireland: problem or opportunity for shale gas extraction?, Appl Geochem. 66 (2016) 82–87.
[44] B.E. Fontenot, L.R. Hunt, Z.L. Hildenbrand, D.D. Carlton Jr., H. Oka, J.L. Walton, D. Hopkins, A. Osorio, B. Bjorndal, Q.H. Hu, K.A. Schug, An evaluation of water quality in private drinking water wells near natural gas extraction sites in the Barnett Shale formation, Environ. Sci. Technol. 47 (2013) 10032–10040.
[45] T. Harada, T. Yatagai, Y. Kawase, Hydroxyl radical generation linked with iron dissolution and dissolved oxygen consumption in zero-valent iron wastewater treatment process, Chem. Eng. J. 303 (2016) 611–620.
[46] L. Bilińska, M. Gmurek, S. Ledakowicz, Comparison between industrial and simulated textile wastewater treatment by AOPs – biodegradability, toxicity and cost assessment, Chem. Eng. J. 306 (2016) 550–559.
[47] G. Boczkaj, A. Fernandes, Wastewater treatment by means of advanced oxidation processes at basic pH conditions: a review, Chem. Eng. J. 320 (2017) 608–633.
[48] S. Miralles-Cuevas, I. Oller, A. Agüera, J.A. Sánchez Pérez, S. Malato, Strategies for reducing cost by using solar photo-Fenton treatment combined with nanofiltration to remove microcontaminants in real municipal effluents: Toxicity and economic assessment, Chem. Eng. J. 318 (2017) 161–170.
[49] S. Jagadevan, M. Jayamurthy, P. Dobson, I.P. Thompson, A novel hybrid nano zerovalent iron initiated oxidation–biological degradation approach for remediation of recalcitrant waste metalworking fluids, Water Res. 46 (2012) 2395–2404.
[50] K. Fukatsu, S. Kokot, Degradation of poly(ethylene oxide) by electro-generated active species in aqueous halide medium, Polym. Degrad. Stab. 72 (2001) 353–359.
[51] R.P. Lattimer, Mass spectral analysis of low-temperature pyrolysis products from poly(ethylene glycol), J. Anal. Appl. Pyrol. 56 (2000) 61–78.
[52] M.D. de Luna, R.M. Briones, C.C. Su, M.C. Lu, Kinetics of acetaminophen degradation by Fenton oxidation in a fluidized-bed reactor, Chemosphere 90 (2013) 1444–1448.
[53] Y.H. Peng, M.K. Chen, Y.H. Shih, Adsorption and sequential degradation of polybrominated diphenyl ethers with zerovalent iron, J. Hazard. Mater. 260 (2013) 844–850.
[54] A.J. Feitz, S.H. Joo, J. Guan, Q. Sun, D.L. Sedlak, T. David Waite, Oxidative transformation of contaminants using colloidal zero-valent iron, Colloids Surf. A: Physicochem. Eng. Aspects 265 (2005) 88–94.
[55] G. Hazel, F. Bucholtz, I.D. Aggarwal, G. Nau, K.J. Ewing, Multivariate analysis of Mid-IR FT-IR spectra of hydrocarbon-contaminated wet soils, Appl. Spectrosc. 51 (1997) 984–989.
[56] G. Socrates, Infrared Characteristic Group Frequencies, Wiley, New York, 1980.
[57] L.J. Bellamy, The Infrared Spectra of Complex Molecules, Chapman and Hall, London, 1980.
[58] L.W. Condie, Target organ toxicology of halocarbons commonly found contaminating drinking water, Sci. Total Environ. 47 (1985) 433–442.
[59] C.H. Weng, Y.T. Lin, C.K. Chang, N. Liu, Decolourization of direct blue 15 by Fenton/ultrasonic process using a zero-valent iron aggregate catalyst, Ultrason. Sonochem. 20 (2013) 970–977.
[60] N.N. Mahamuni, Y.G. Adewuyi, Advanced oxidation processes (AOPs) involving ultrasound for waste water treatment: a review with emphasis on cost estimation, Ultrason. Sonochem. 17 (2010) 990–1003.
[61] B. Kiril Mert, T. Yonar, M. Yalili Kilic, K. Kestioglu, Pre-treatment studies on olive oil mill effluent using physicochemical, Fenton and Fenton-like oxidations processes, J. Hazard. Mater. 174 (2010) 122–128.
[62] D. Huang, C. Hu, G. Zeng, M. Cheng, P. Xu, X. Gong, R. Wang, W. Xue, Combination of Fenton processes and biotreatment for wastewater treatment and soil remediation, Sci. Total Environ. 574 (2017) 1599–1610.
[63] J.R. Bolton, K.G. Bircher, W. Tumas, C.A. Tolman, Figures-of-Merit for the technical development and application of advanced oxidation processes, J. Adv. Oxid. Technol. 1 (1996).
[64] B. Kiril Mert, T. Yonar, M. Yalili Kiliç, K. Kestioğlu, Pre-treatment studies on olive oil mill effluent using physicochemical, Fenton and Fenton-like oxidations processes, J. Hazard. Mater. 174 (2010) 122–128.